Chapter-4

Efficient Removal of Congo Red from Aqueous Solutions Using Calcined and Uncalcined MgZnFe-CO_3 Ternary Layered Double Hydroxide

4.1. Abstract

This study investigates the textile industries' dye Congo-red removal from aqueous solution using the calcined and uncalcined $[Mg_{0.5}^{2+}Zn_{0.25}^{2+}Fe_{0.25}^{3+}(OH)_2].(CO_3^{2-})_{0.125}.H_2O$ or MgZnFe-CO_3 ternary layered double hydroxide (LDH). XRD confirms the successful formation of the crystalline structure of LDH. FTIR analysis shows that the peak position at 1108 cm^{-1}, which indicates the presence of $S = O$ group. TEM analysis reveals the formation of a hexagonal shape morphology, whereas BET measurements demonstrate an improvement in surface area after calcination. This study analyzed dye adsorption, which is affected by interaction time, solution pH, and adsorbent dosage. The adsorption data is analyzed using the Langmuir isotherm and Freundlich isotherm, while the kinetics data is analyzed using pseudo-first-order, pseudo-second-order, and intraparticle diffusion models. The change in enthalpy (ΔH_0) being positive and the change in Gibbs free energy (ΔG_0) being negative designates that the adsorption process is endothermic and occurs spontaneously. The Langmuir isotherm model analyzed the adsorption isotherm data and calculated the amount of adsorbate adsorbed by adsorbent. The maximum amount of Congo-red adsorbed by calcined and uncalcined layered double hydroxide are 205.76 and 89.76 mg/g. These results suggested that calcined layered double hydroxide is a significant adsorbent for removing effluents from wastewater.

4.2. Results and discussion

4.2.1. Characterization

4.2.1.1. X-ray diffraction analysis

The x-ray diffraction of uncalcined, calcined LDH is represented in Figure 4.1. All peaks of uncalcined material located 2θ as 11.39°, 22.90°, 34.14°, 38.52°, 45.78°, 59.34°, 60.70° represents (003), (006), (009), (015), (018), (110) and (113) reflection peaks. Some additional peaks are coming due to the ageing temperature. The peaks position located at 2θ is 31.76°, 36.29°, 47.55°, 51.72°, 54.89° and 56.60° represents

the (310), (330), (104), (510), (620) and (251) reflection peaks. All these peaks correspond to iron oxide hydroxide due to ageing

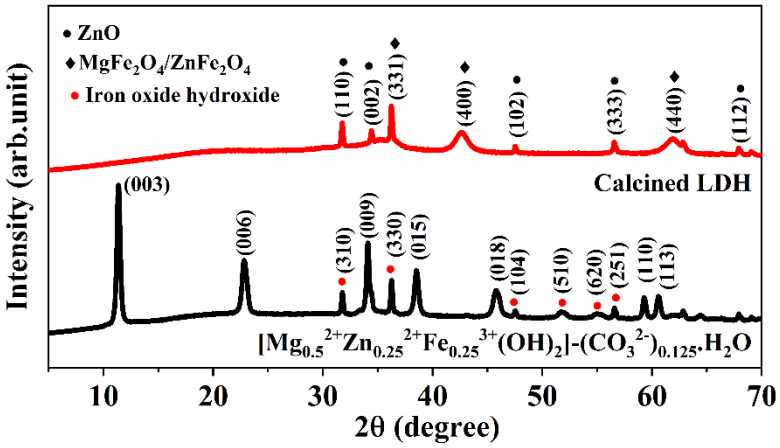

Figure 4.1: X-ray diffraction spectra of (a) MgZnFe-CO_3 LDH (b) calcined MgZnFe-CO_3 LDH.

temperature (JCPDS NO. 22-0353, 34-1266, 75-1594). Most peaks vanish due to heat treatment, and the material becomes an amorphous structure. After calcination, the broad and weak intense peaks of $MgFe_2O_4$ and $ZnFe_2O_4$ were observed [171].

From the material synthesis point of view, one of the important limitations of the present study was not obtaining the pure phase of LDH. However, the planned

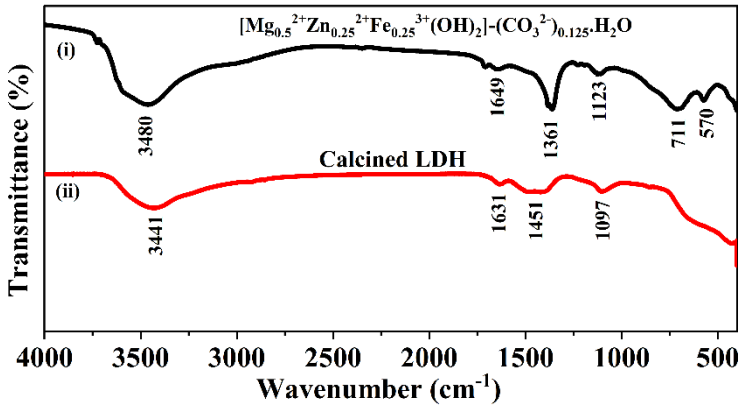

Figure 4.2: Fourier transformed infrared spectra of (a) MgZnFe-CO_3 LDH (b) calcined MgZnFe-CO_3 LDH.

application of the synthesised material was the adsorption of dyes, so this limitation

was not so important. Maintaining the desired temperature during the synthesis of the material was another limitation.

4.2.1.2. Fourier Transform Infrared spectrum analysis

The Fourier Transform Infrared of the uncalcined, calcined and after CR adsorption by calcined LDH is given in Figure 4.2. In Figure 2(i), the broad and high intense peak at 3480 cm^{-1} and low intense peak at 1361 cm^{-1} represents the bending vibration of interlayer water and stretching vibration peak of $-OH$, which become less intense for

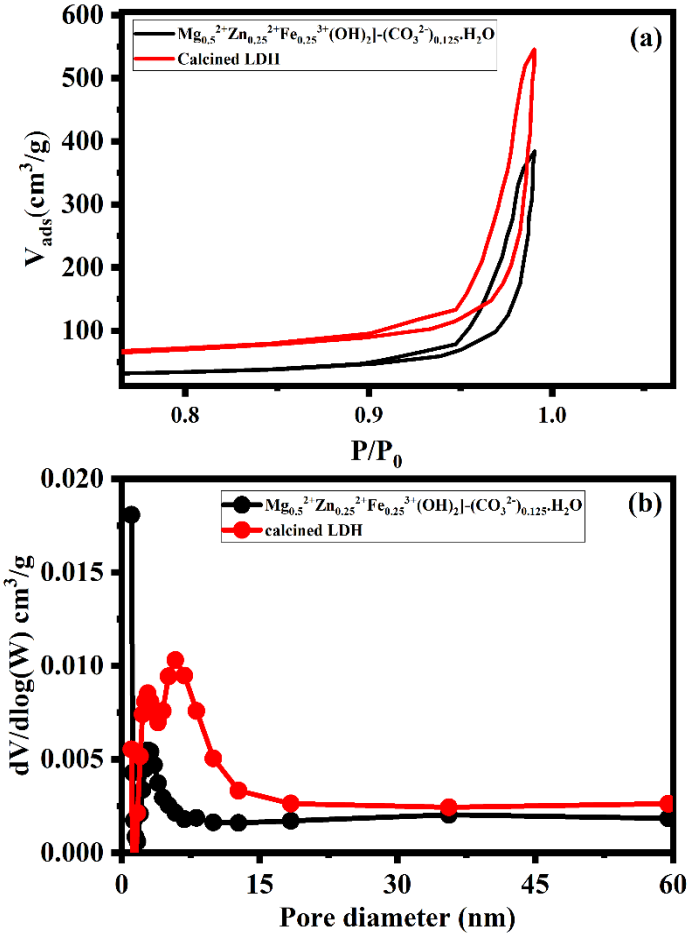

Figure 4.3: (a) N_2 adsorption-desorption isotherms and (b) the corresponding pore size distribution curve for MgZnFe-CO_3 LDH and calcined MgZnFe-CO_3 LDH.

calcined LDH by heat treatment and slightly shifts the peak and shows around at 3441 and 1631 cm^{-1}. The sharp and highly intense peak near around 1361 cm^{-1} exhibits the intercalated CO_3^{2-} anion and become less intense and slightly shifted due to high

calcined temperature but did not wholly vanish of intercalated anions. This finding is discussed in previous literature indicating the whole intercalated anion completely vanishes above the temperature 700 °C. The peak is in the range of 500 to 1000 cm^{-1} is allotted to the $M-O-M$ (Where M = Mg, Zn and Al) [172,173].

4.2.1.3. N_2 adsorption-desorption analysis

The N_2 adsorption-desorption and pore size distribution of uncalcined and calcined LDH are shown in Figure 4.3. According to the previous study, these materials displayed type I isotherm, according to the classification of G Leofanti et al. [174]. In Figure 4.3a, this isotherm exhibits an H3 type of hysteresis loop at high pressure. This type of hysteresis is found on solids containing aggregates or agglomerates of particles of slit-shaped pores with unequal size or shape. This type of hysteresis is consistent with porous and microporous material. The pore distribution curve nature for both samples is the same, with a range of up to 6 nm.

Table 4.1. Textural properties of the samples

Name	Surface area (m^2/g)	Average pore diameter (nm)	Pore volume (cm^3/g)
MgZnFe-CO_3 LDH	51.9	34.79	0.579
Calcined MgZnFe-CO_3 LDH	93.6	32.75	0.801

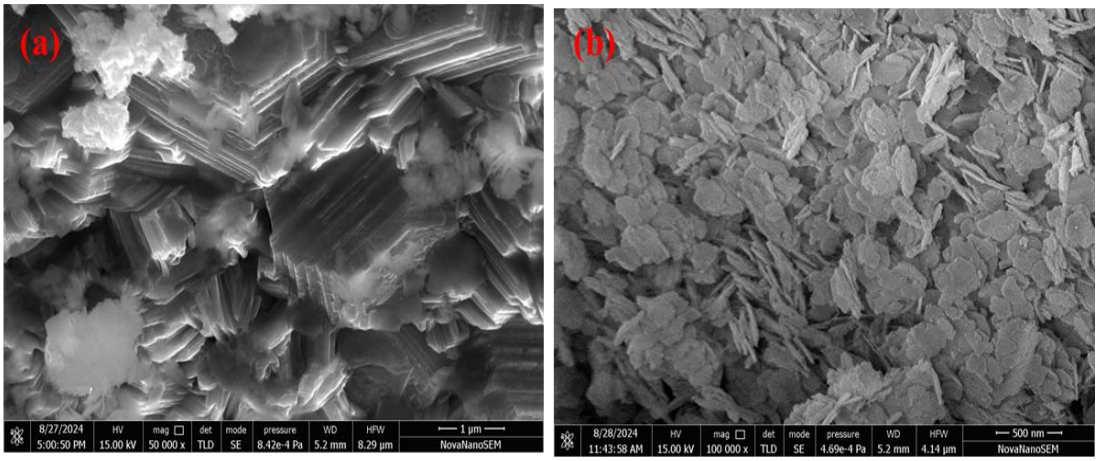

Figure 4.4: SEM images of (a) uncalcined MgZnFe-CO_3 LDH, (b) calcined MgZnFe-CO_3 LDH.

The textural properties of both materials are listed in Table 4.1. The surface area of MgZnFe-CO_3 increase from 51.9 to 93.6 $^{m^2}/_{g}$ and the pore volume from 0.579 to 0.801 $^{cm^3}/_{g}$ by the heat treatment of the material at 500 °C for 4h. Water and anion molecules are eliminated at the calcination temperature, which makes it easier to create channels and porous structures that may increase pore volume and specific surface area.

4.2.1.4. SEM and TEM analysis

The scanning electron microscopy images of the uncalcined and calcined LDH are shown in Figure 4.4. This figure demonstrated that the surface morphology of the LDH exhibits a layered structure. The particles appear to be of varying sizes and tend to form agglomerates. The surface morphology became rough and destroyed the layered structure after calcined the LDH. The transmission electron microscope observed the surface morphology of the material. TEM images were taken at a higher and lower magnification of the system in the scale range of micrometre to nanometre, as shown in Figure 4.5. Four images acquired at different magnifications demonstrate the hexagonal morphology yet exhibit agglomeration in disparate configurations [175].

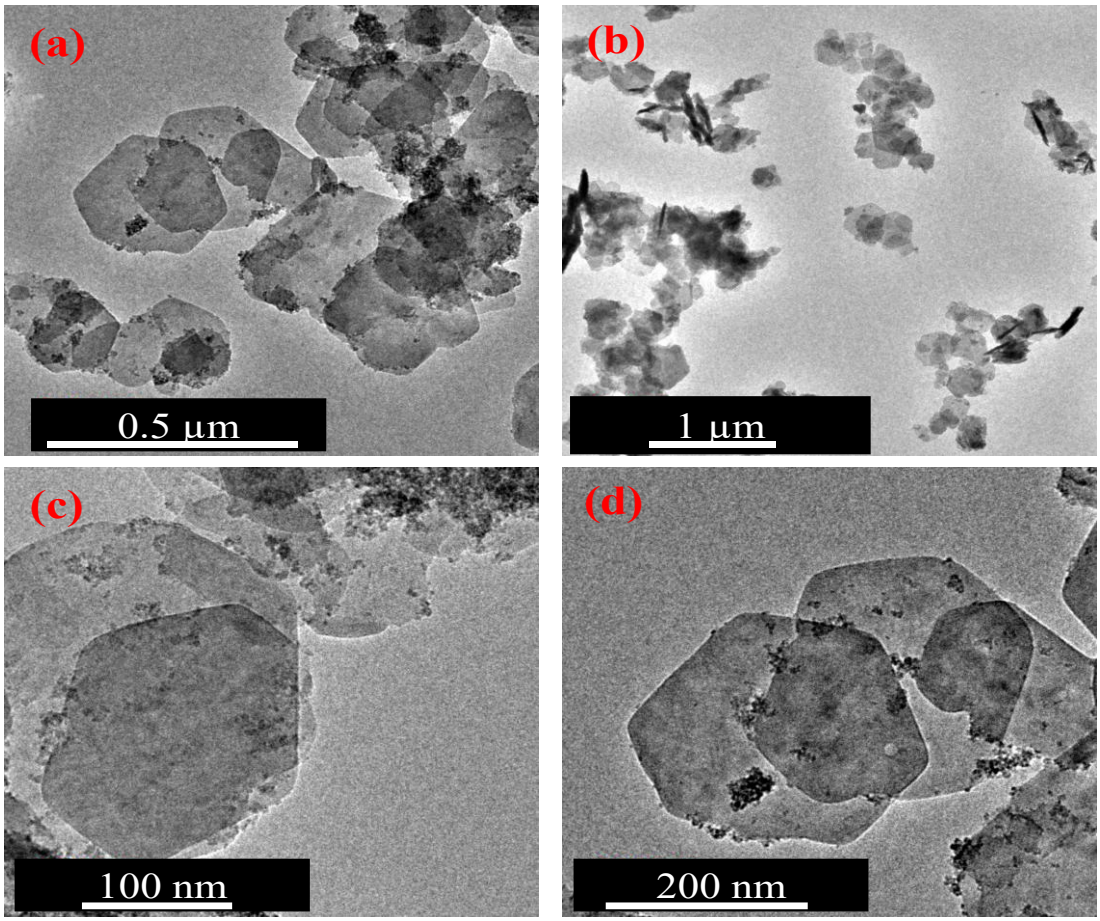

Figure 4.5: TEM images of MgZnFe-CO_3 layered double hydroxide at different resolutions (d is the zoomed version of a).

4.2.1.5. X-ray Photoelectron Spectroscopy (XPS)

X-ray photoelectron spectroscopy (XPS) is a powerful technique that detects the ionisation state of the element, which is present in the experimental materials. The XPS spectra were recorded using a Thermo Fisher Scientific K-Alpha XPS system (Thermo

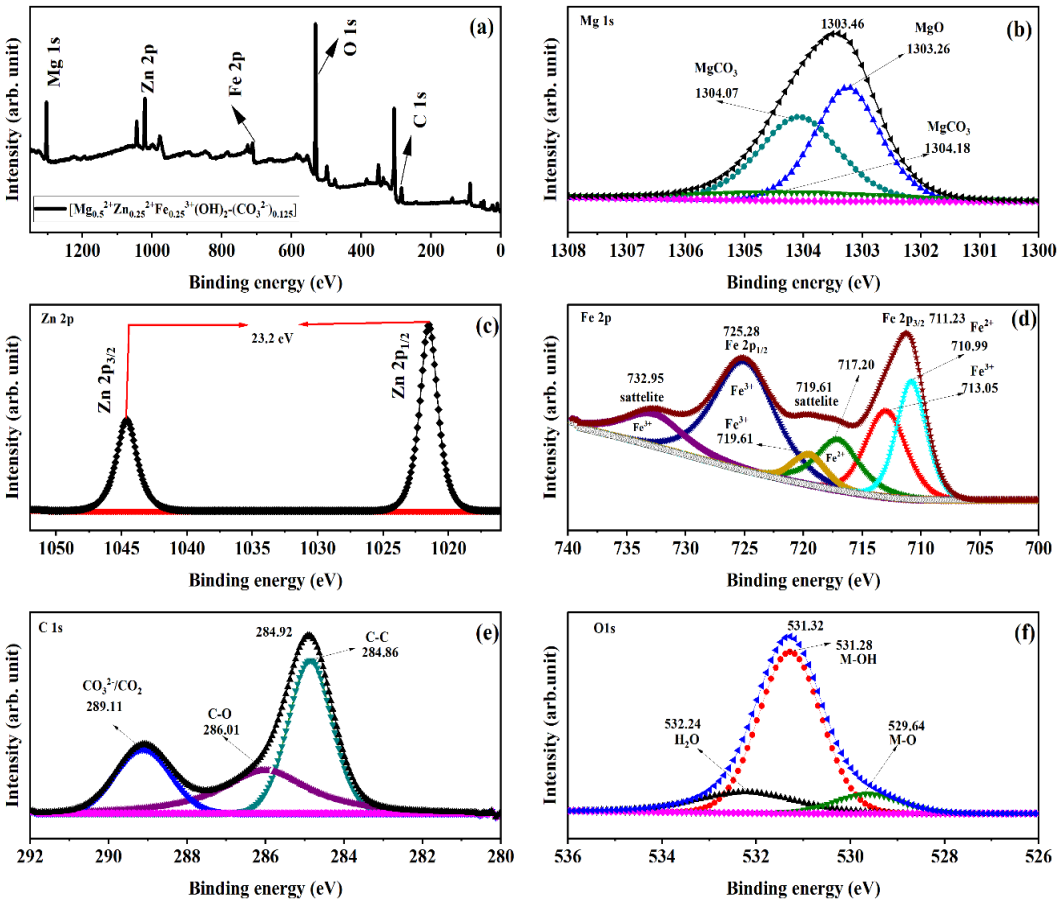

Figure 4.6: XPS spectra of (a) MgZnFe-CO_3 LDH (b) Mg 1s (c) Zn 2p (d) Fe 2p (e) C 1s (f) O 1s.

Fisher Scientific, UK) equipped with a micro-focused monochromatic Al Kα X-ray source at 1486.68 eV. The XPS analysis determined the composition and valence states on the LDH's surface. The present elements of calcined and uncalcined LDH are shown in Figure 4.6 and 4.7. The XPS spectra confirmed the presence of Mg, Zn, Fe, C and O. The XPS spectra for uncalcined LDH reveal an Mg 1s peak centered at 1303.46 eV. The Mg 1s peaks observed at 1304.6-1304.7 eV are associated with $MgCO_3$. MgO was detected on the surface material at 1303.26 eV [176]. The Zn 2p peaks, located at 1021.49 eV and 1044.64 eV, represent $Zn\ 2p_{1/2}$ and $Zn\ 2p_{3/2}$, respectively. The

estimated spin-orbit splitting between $Zn\ 2p_{1/2}$ and $Zn\ 2p_{3/2}$ (ΔZn) was 23.15 eV, matching the expected value for Zn^{2+} [177].

The $Fe\ 2p_{3/2}$ and $2p_{1/2}$ peaks are observed at binding energies of 711.23 eV and 725.28 eV, respectively, indicating Fe^{2+} and Fe^{3+}. The satellite peaks at 732.95 eV and 719.61 eV are associated with Fe^{3+}. Peaks at 710.99 and 717.20 eV are attributed to Fe^{2+}, while the peak at 713.05 eV corresponds to Fe^{3+} [178,179]. The C1s spectra reveal peaks at 284.86 eV, 286.01 eV, and 289.11 eV, corresponding to $C-C$, $C-O$, and CO_3^{2-}, CO_2 respectively [180]. The O1s spectra show peaks at 529.64 eV, 531.28 eV, and 532.24 eV, which correspond to $M-O$, $M-OH$ (where $M = Mg, Zn, Fe$), and H_2O (surface water), respectively [181].

The XPS spectra of calcined LDH is shown in Figure 4.7. This spectrum reveals Mg 1s peaks centered at 1303.59 eV, with peaks observed between 1303.17 and 1303.66 eV

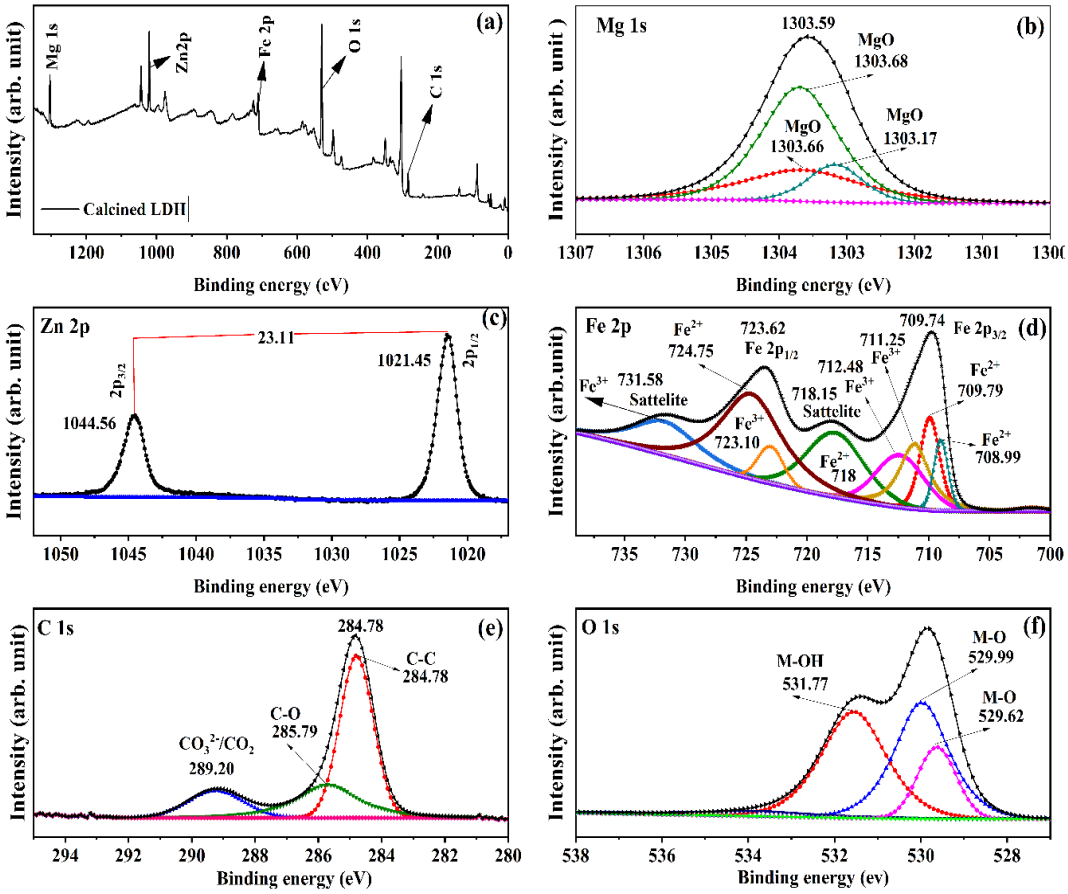

Figure 4.7: XPS spectra of (a) calcined MgZnFe-CO_3 LDH (b) Mg 1s (c) Zn 2p (d) Fe 2p (e) C 1s (f) O 1s.

corresponding to MgO [182]. The Zn 2p peaks detected at 1021.45 eV and 1044.56 eV correspond to $Zn\ 2p_{1/2}$ and $Zn\ 2p_{3/2}$, respectively. The spin-orbit splitting between $Zn\ 2p_{1/2}$ and $Zn\ 2p_{3/2}$ (ΔZn) was 23.15 eV, which corresponds with the expected value for Zn^{2+} [177]. The main peaks for Fe 2p3/2 and 2p1/2 are detected at binding energies of 709.74 eV and 723.62 eV, respectively, with satellite peaks at 731.58 eV and 718.15 eV corresponding to Fe^{3+} and Fe^{2+}. The peak positions are at 711.25 eV, 712.48 eV, and 723.10 eV, corresponding to Fe^{3+}, while the peaks at 708.99 eV, 709.79 eV and 724.75 eV indicate Fe^{2+} [178,179]. The C1s spectrum shows binding energy peaks at 284.78 eV, 285.79 eV, and 289.20 eV, corresponding to $C-C$, $C-O$, and CO_3^{2-}/CO_2 respectively [180]. The O1s spectra show the peaks at 592.62 eV, 529.99 eV, and 531.77 eV represent $M-O$, $M-OH$ (where $M = Mg, Zn, Fe$) [181].

4.2.2. Kinetic studies

4.2.2.1. The pH effects

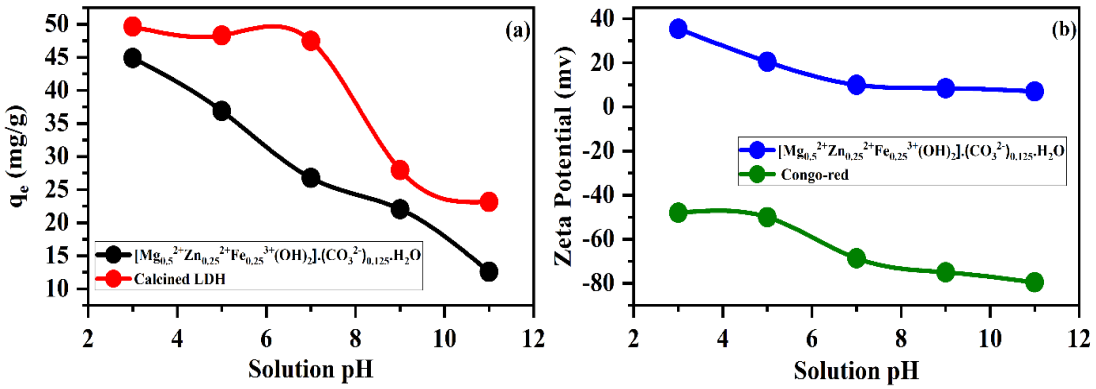

Figure 4.8: (a) Effect of adsorption capacity at different pH onto the calcined and uncalcined LDH (V_0= 25 ml, m= 15 mg) (b) Zeta potential of MgZnFe-CO_3 LDH and CR.

The pH effect is one of the most crucial parts of adsorption. The amount of dye was adsorbed, and the zeta potential of the dye and LDH at various pH is represented in Figure 4.8. It was observed that the removal capacity was high at pH 3 and that the CR adsorption capacity decreased with the increase in the solution pH. The pH of the dye solution significantly influences the adsorption capacity, as it affects the charge of dye molecules and the layered double hydroxide in the aqueous solution. The CR is an anionic dye, but the surface charge changes with different pH changes. The adsorption capacity by the LDH is highest at pH 3, but it decreases with the increase of solution

pH. The behaviours can be clarified based on the surface charge of the material and CR solution. In an acidic medium, the surface charge becomes more positive by adsorbing H^+ ions from the solution, which interacts with the sulfonyl groups (SO_3^-) of the anionic CR molecules. At pH 5, the surface charge is less than at pH 3, leading to a lower adsorption capacity of the material at pH 5 compared to pH 3. In an alkaline medium, both the material and CR dye acquire a more negative charge by adsorbing OH^- ions, which leads to electrostatic repulsion, making the adsorption of CR dye less favorable. Consequently, pH 10 produced the lowest adsorption capacity.

4.2.2.2. Effect of time

The Congo-red adsorption onto the calcined and uncalcined LDH as a function of contact time at normal pH and temperature 298 K, with dye concentration (50 to 150 mg/L) is shown in Figure 4.9. In this figure, CR adsorption on LDH reached equilibrium at a concentration of 50 mg/L after 80 minutes, and as the contact time increased, it reached its maximum adsorption percentage. The CR adsorption onto calcined LDH

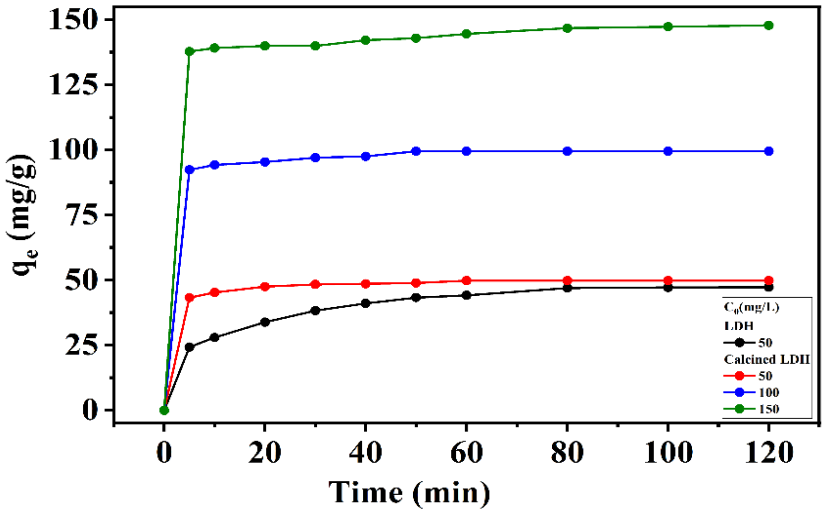

Figure 4.9: Effect of contact time and initial concentration in the adsorption of CR onto the two samples (V_0 = 50 ml, m= 50 mg, pH=7).

reached equilibrium in 30 minutes and maintained its maximum adsorption as the contact time duration increased, i.e., it is highly efficient compared to LDH. These results proved that the calcined LDH has a higher affinity for adsorbing the dye from the aqueous solution than the uncalcined LDH. The fast removal efficiency of CR onto

the two materials related to surface complexation or chemical adsorption is the primary mechanism [183]. Before the material was saturated, the CR adsorption was observed to occur in two steps, as seen in Figure 4.9. The first step was extremely sharp, and the second step slowly rose relatively and reached equilibrium. The material's surface contains numerous active sites, facilitating rapid adsorption in the first step. In the second step, the active sites were saturated, preventing other CR molecules from adhering to the adsorbent surface, which caused the adsorption to slow down [184].

4.2.2.3. Effect of dosage

Influence of adsorbent dosage on the removal efficiency percentage for CR adsorption, as depicted in Figure 4.10. The percentage of Congo-red adsorption increased from 44.72 % to 98.99 % as the material amount was raised from 0.1 to 0.8 g/L. Therefore,

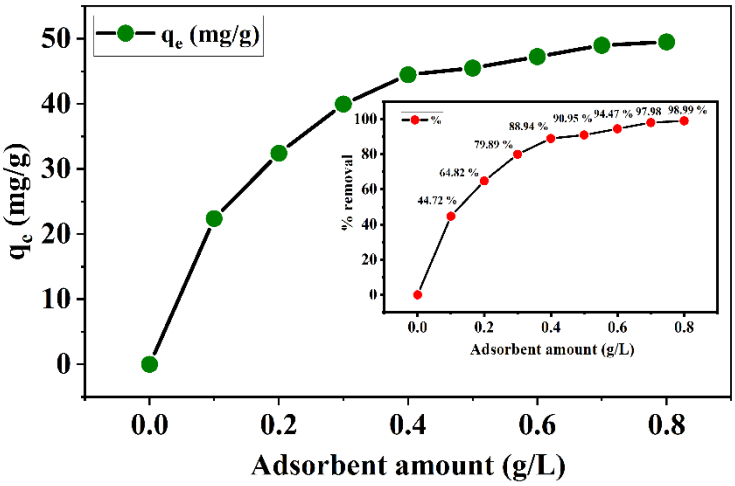

Figure 4.10: Effect of adsorbent dose of CR adsorption onto the calcined LDH (V_0 = 50 ml, pH=7).

maximum CR adsorption occurred because more adsorption sites are available at higher doses.

4.2.3. Adsorption isotherm

4.2.3.1. Langmuir and Freundlich isotherm

The adsorption isotherm is one of the most important isotherms for understanding the interaction between the adsorbate and adsorbent. Langmuir and Freundlich, two well-known isotherm models, were involved in analyzing the adsorption isotherm data. As per the Langmuir isotherm model, adsorption occurs through the monolayer formation

of adsorbate molecules on the homogeneous surface of the adsorbent. The linear form of Langmuir isotherm model can be expressed [185]

$$\frac{C_e}{q_e} = \frac{1}{(K_L \times q_m)} + \frac{C_e}{q_m} \quad \ldots\ldots\ldots\ldots\ldots\ldots\ldots\ldots (4)$$

Where q_e(mg/g) and C_e(mg/L) is the equilibrium adsorption capacity and equilibrium concentration of adsorbate molecules. q_m(mg/g) is the maximum adsorption capacity of the adsorbent, while K_L (L/mg) is the Langmuir constant. The dimensional separation

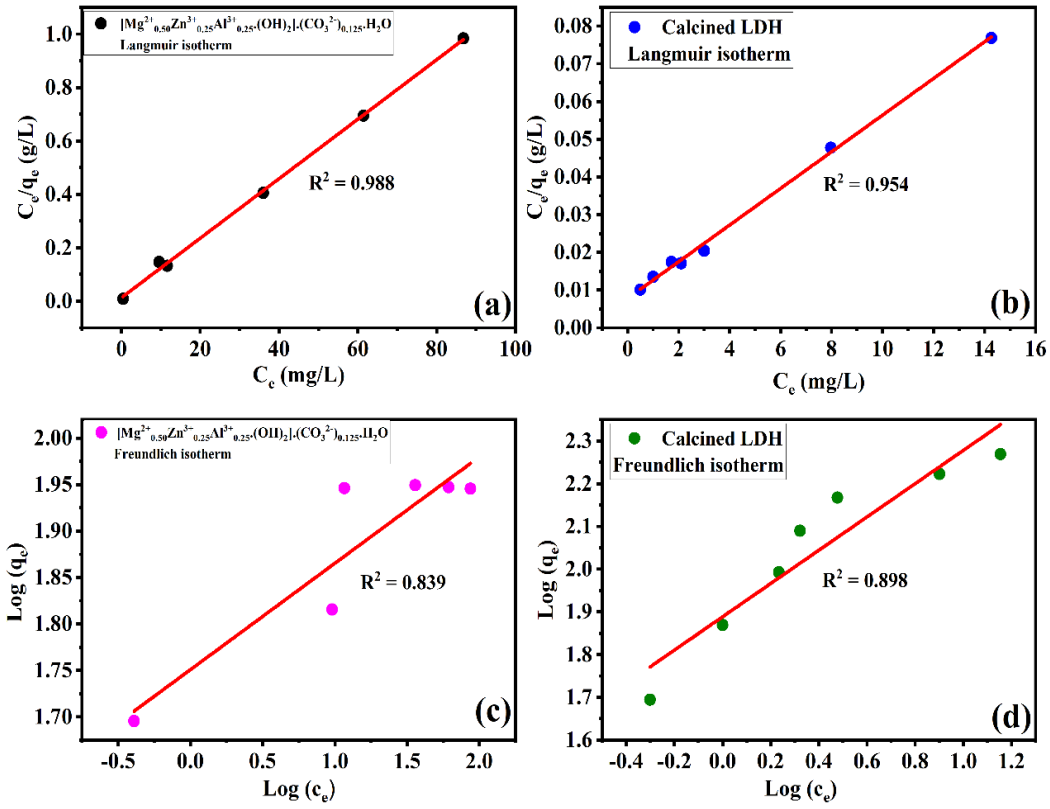

Figure 4.11: Langmuir isotherm and Freundlich isotherm of (a &c) MgZnFe-CO_3 LDH (b &d) calcined MgZnFe-CO_3 LDH, the line indicates the linear fitting, dot indicates the experimental value (R^2 of Langmuir isotherm is greater than Freundlich isotherm, Langmuir isotherm model is applicable).

factor can interpret the nature of the adsorption process R_L as

$$R_L = \frac{1}{1+K_L C_0} \ldots\ldots\ldots\ldots\ldots\ldots (5)$$

When $R_L = 0$, suggest that the adsorption is irreversible. The process is favourable when the value of R_L in the range of $0 < R_L < 1$ and unfavourable $R_L > 1$. The adsorption is established to have a linear relationship when the value of $R_L = 1$ [186].

The Freundlich isotherm model defines a surface of heterogeneity through a non-ideal and reversible adsorption process, and it can be formulated as follows.

$$\mathrm{Log}(q_e) = \mathrm{Log}(K_f) + \frac{1}{n}\mathrm{Log}(C_e)$$

$$\text{or } q_e = K_f C_e^{\frac{1}{n}} \quad \ldots\ldots\ldots\ldots\ldots\ldots (6)$$

The curve is plotted against $\mathrm{Log}(q_e)$ vs $\mathrm{Log}(C_e)$ gives the value of K_f and n. Where K_f represents the Freundlich constant, and n is the intensity factor or the surface heterogeneity. Where the value of n indicates whether the adsorption is complex ($n <$ 1), partially difficult ($1 \leq n < 2$), or easy ($2 \leq n < 10$) [187].

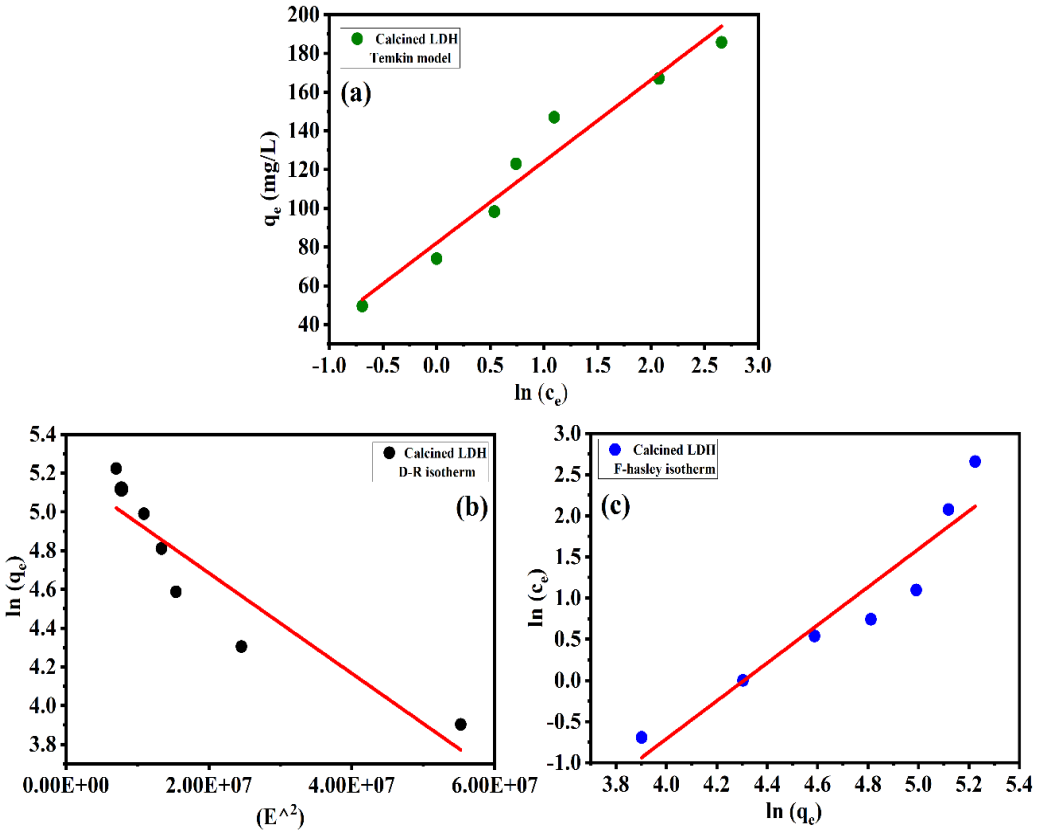

Figure 4.12: Congo red adsorption on calcined MgZnFe-CO_3 LDH (a) Temkin isotherm (b) D-R isotherm (c) F-hasley isotherm onto the calcined MgZnFe-CO_3 LDH, dot indicates the experimental value and line represents the linear fitting.

Figure (4.11) shows the fitted data of both isotherm models, as shown in Table 4.2. The correlation coefficient R^2 confirmed the suitable fitted model to discuss the adsorption isotherm. In Table 4.2, R^2 of Langmuir isotherm model is bigger than the Freundlich isotherm model. So, the Langmuir isotherm model is appropriate for discussing CR adsorption onto the material's surface.

Table 4.2: Langmuir and Freundlich isotherm model constant and correlation coefficient for Congo-red adsorption onto the calcined and uncalcined MgZnFe-CO_3 layered double hydroxide surface.

Model Name	MgZnFe-CO_3 LDH	Calcined MgZnFe-CO_3 LDH
Langmuir isotherm	$\mathbf{q_m = 89.76\ mg/g}$ $\mathbf{K_L = 0.881\ L/mg}$ $\mathbf{R^2 = 0.988}$	$\mathbf{q_m = 205.76\ mg/g}$ $\mathbf{K_L = 0.623\ L/mg}$ $\mathbf{R^2 = 0.954}$
Freundlich isotherm	$\mathbf{K_f = 56.33\ mg/g}$ $\mathbf{n = 8.73}$ $\mathbf{\frac{1}{n} = 0.114}$ $\mathbf{R^2 = 0.839}$	$\mathbf{K_f = 77.34\ mg/g}$ $\mathbf{n = 2.56}$ $\mathbf{\frac{1}{n} = 0.389}$ $\mathbf{R^2 = 0.898}$

4.2.3.2. Temkin isotherm model

This model examines the heat of the adsorbate-adsorbent interaction and presumes a multilayer formation between them during adsorption. This isotherm model is worried about the decline of the heat of adsorption as a function of temperature, which is a linear relationship. The linear form of Temkin isotherm can be written as [188,189].

$$q_e = \frac{RT}{b} lnc_e + \frac{RT}{b} lnK_m \ldots\ldots\ldots\ldots\ldots\ldots (7)$$

Where R is the gas constant in J/ (mol. K), T is the temperature in K, b is the Temkin constant correlated with the adsorption heat in J/mol, and K_m is the Temkin isotherm constant in L/g. According to this isotherm, the heat of adsorption of each molecule in the layer decreases with the surface area covered logarithmically rather than linearly. The isotherm model can predict the gas-phase equilibria rather than the liquid phase. The linear plot of lnc_e vs q_e is shown in Figure 4.12a. The Temkin model constants values are shown in Table 4.3. The adsorption energy obtained for adsorption is 60.69

J/mg, which indicates that the adsorption is endothermic, i.e., a strong adsorbate-adsorbent interaction was occurring. This value suggests that chemisorption occurs between the adsorbent and adsorbate during adsorption, aligning with the pseudo-second-order kinetics model.

Table 4.3: Adsorption isotherms parameters of Congo-red over the calcined MgZnFe-CO_3 layered double hydroxide

Adsorption Models	Parameter values
Temkin model	b = 58.87 J/mol, $K_m = 3.86$ L/g.
Dubinin-Radushkevich model	B ($J^2/_{mol^2}$) = 1.5 $\times 10^{-7}$ E = 1770 (J/mol). Q_m= 145 mg/g.

4.2.3.3. The Dubinin-Radushkevich isotherm model

This model gives information about the material's porosity and estimates adsorption energy. This isotherm model presumes the heterogeneous surface and variation of the adsorption potential during the adsorption process. Figure 4.12b represents the linear equation between the E^2 vs lnq_e. The energy value of 3.66 KJ/mol confirms that there has been a physisorption interaction between the adsorbent and adsorbate.

4.2.3.4. Haseley isotherm model

This isotherm model provides evidence that multilayers are forming on the solid surface. Figure 4.12c represents the linear plot lnq_e vs lnc_e with a slope n and intercept lnK. The nature of the plot (linear) confirms the viable phenomenon of a multilayer of dye molecules on calcined layered double hydroxide. This model fitted the data and ensured the adsorbent surface was heterosporous.

4.2.4. Kinetics model of Adsorption isotherm

Adsorption kinetics are crucial in adsorption processes to predict the mass transfer process occurring. The adsorption is significantly faster than the internal and external diffusion. It shows that after a few minutes, the adsorption was saturated. However, the long-range equilibrium time proposes that the reaction rate is controlled by internal diffusion. Adsorption kinetics are essential because they predict the rate at which pollutants are eliminated from an aqueous solution. The resulting data also provides

information about the mechanism of the adsorption. Many models are accessible for examining the adsorption kinetics data, such as pseudo-first-order, pseudo-second-order, and intraparticle diffusion models.

The pseudo-second-order kinetics model can be written as [185]

$$\frac{t}{q_t} = \frac{1}{k_2 q_e^2} - \frac{1}{q_e} t \ldots\ldots\ldots\ldots\ldots\ldots\ldots\ldots (8)$$

The following equation can express the pseudo-first-order kinetics model.

$$log(q_e - q_t) = log q_e - k_1 t \ldots\ldots\ldots\ldots\ldots\ldots\ldots\ldots (9)$$

These two models fit the adsorption kinetics data; the results are listed in Table 4.4. The correlation coefficient R^2 expressed the model-calculated data and experimental data. Where k_1, k_2 is pseudo-first-order and pseudo-second-order rate constant. The linear form of pseudo-first-order (Figure 4.14) and pseudo-second-order kinetic model is shown in Figure 4.13.

Table 4.4. Kinetic model parameters obtained in the adsorption of Congo-red onto the calcined and uncalcined MgZnFe-CO_3 layered double hydroxide pseudo-second-order and pseudo-first-order.

Initial concentration of congo-red c_0(mg/L)	**$q_{e,exp}$ (mg/g)**	**Pseudo-second-order**			**Pseudo-first-order**		
		$q_{e,cal}$ (mg/g)	**$k_2(10^{-4})$**	**R^2**	**$q_{e,cal}$ (mg/g)**	**$k_1(10^{-4})$**	**R^2**
Calcined MgZnFe-CO_3 LDH							
50	49.50	49.43	343	0.999	3.35	-2.08	0.775
100	99.40	99.60	203	0.999	4.71	-2.83	0.752
150	148.50	148.80	67	0.999	14.76	-2.95	0.969
MgZnFe-CO_3 LDH							
50	48.50	50.22	29	0.995	30.11	-25.41	0.994

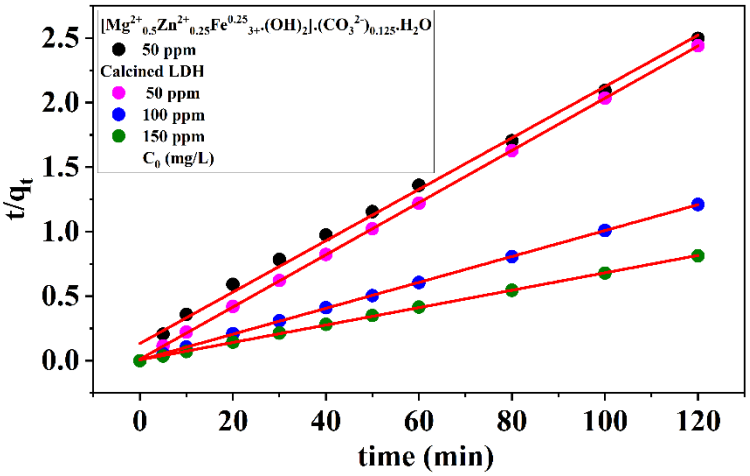

Figure 4.13: Pseudo-second-order model of congo-red adsorption onto the calcined and uncalcined MgZnFe-CO_3 layered double hydroxide, line indicates the linear fitting and dot indicates the experimental value.

The rate constant of the pseudo-first-order and pseudo-second-order kinetics model decreases from $-2.08 \times 10^{-4} to - 2.95 \times 10^{-4}\ min^{-1}$and $343 \times 10^{-4}\ to\ 67 \times 10^{-4}\ min^{-1}$ with the increasing dye concentration, is shown in Table 4.4. The correlation coefficient R^2 of the pseudo-first-order model is lower than the pseudo-second-order model. These results confirmed the poor pseudo-first order fit for experimental and calculated data, whereas, for the pseudo-second model, the calculated and experimental data are closely matched. These results confirmed that the pseudo-second-order is appropriate for discussing CR adsorption onto the material.

The pseudo-second-order model is consistent with a chemisorption mechanism as the rate-determining step and is dependent on the adsorption loading on the solid phase. The pseudo-second-order model also has the benefit of being able to predict behaviours across the entire range of the adsorption process [190].

The intra-particle diffusion model, suggested by Weber and Morris, is used to investigate the diffusion of Congo-red onto the material.

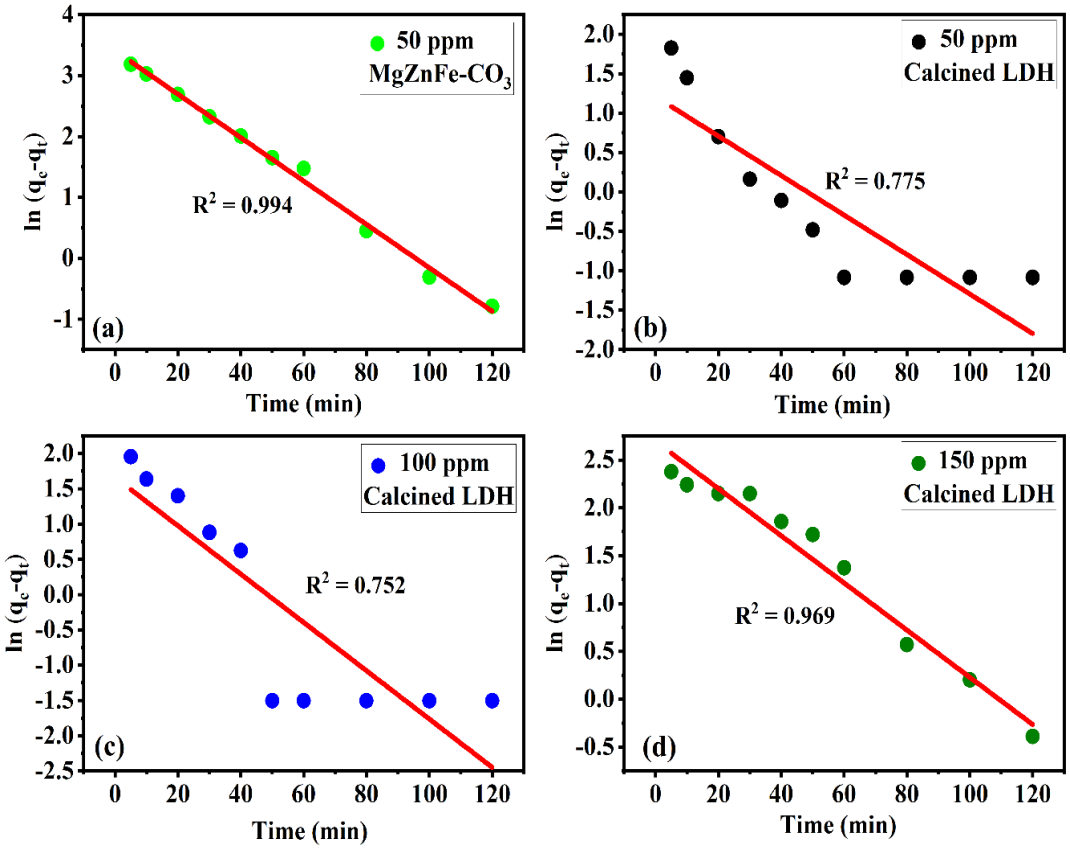

Figure 4.14: Pseudo-first-order model of congo-red adsorption onto the calcined and uncalcined MgZnFe-CO_3 layered double hydroxide for (a) MgZnFe-CO_3 (b, c & d) calcined LDH. Line indicates the linear fitting and dot indicates the experimental value. Not fitted well (R^2 of pseudo first order is less than the R^2 of pseudo second order model).

The linear equation is $q_t = k_1 t^{1/2} + C$..... (10)

In the equation $k_1(\frac{mg}{gmin^{-1}})$ is the diffusion rate constant, and C (mg/g) is the intercept. The plot of the q_t vs $t^{1/2}$ as shown in Figure 4.15. The intra-particle diffusion controls

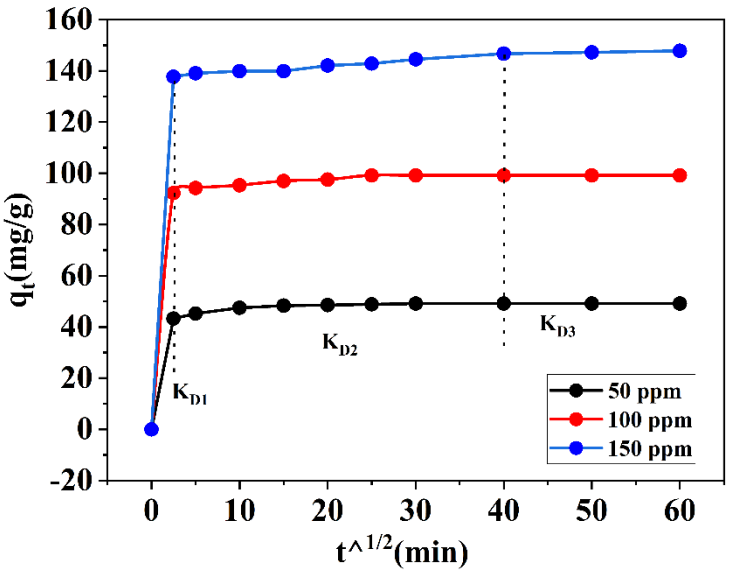

Figure 4.15: Intra-particle diffusion model of Congo-red adsorption onto the calcined MgZnFe-CO_3 layered double hydroxide (ppm=mg/L).

adsorption if this plot meets the linear equation and the experimental data passes through the origin in a straight line. Otherwise, the adsorption process is multistep if it is not a linear formation. The first, sharper portion exhibits the external diffusion of Congo-red molecules on the material surface. The second straight line portion is the slow equilibrium stage with intra-particle diffusion through the mesoporous system of the particle. The findings lead us to believe that the dye adsorption process involves multiple steps.

4.2.5. Adsorption thermodynamics

The thermodynamics parameters such as Gibbs free energy change (ΔG_0), enthalpy change (ΔH_0) and entropy change (ΔS_0) were also investigated with the changes of temperature in the adsorption process. This process was performed to define the type of the adsorption process, i.e. endothermic or exothermic, spontaneous, or nonspontaneous. The experiments were observed using Congo-red concentration 50 mg/L and 25 mg of calcined LDH at 25 °C, 35 °C and 45 $\pm$1 °C. The values of thermodynamic parameters such as ΔH_0 and ΔS_0 were calculated following the equation

$$lnK_d = \frac{\Delta S^0}{R} - \frac{\Delta H^0}{RT} \quad \ldots\ldots\ldots\ldots\ldots\ldots (11)$$

$$K_d = \frac{q_e}{C_e} \ldots\ldots\ldots\ldots\ldots\ldots\ldots\ldots\ldots (12)$$

Where K_d is the distribution coefficient, R is the gas constant, and T is the temperature (K). Figure 4.16 shows the plot of lnK_d vs 1/T gives the value of slope and intercept, which corresponds to $\frac{\Delta H^0}{R}$ and $\frac{\Delta S^0}{R}$ respectively. ΔG_0 is calculated using the following equation

$$\Delta G_0 = \Delta H_0 - T\Delta S_0 \ldots\ldots\ldots\ldots\ldots\ldots (13)$$

The thermodynamic parameters from the temperature dependence isotherm are listed in Table 4.5. These values prove that the negative value of ΔG_0 increases with the temperature increase, i.e., the adsorption process becomes spontaneous at high temperatures. The change in enthalpy ΔH_0, is positive, indicating that the adsorption process is endothermic or physical. The positive value of change of entropy ΔS_0, indicates that at high temperatures, the adsorption becomes more random on the surface of the adsorbent/adsorbate interface [191].

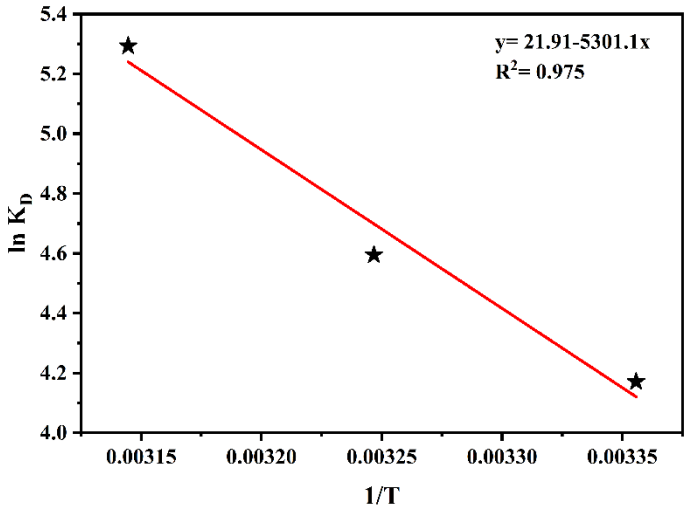

Figure 4.16: Van't plot for the adsorption of Congo-red on calcined MgZnFe-CO_3 layered double hydroxide, red line is fitting line and star sign is experimental value.

Table 4.5: Thermodynamic parameters for adsorption of Congo-red onto the calcined MgZnFe-CO_3 LDH

Temperature (K)	ΔG_0(KJ/mol)	ΔH_0(KJ/mol)	ΔS_0(J/mol. K)
298	-54.23	44.07	182.15
308	-56.05		
318	-57.87		

Table 4.6 shows the adsorption capacities of the prepared materials, as well as those of some previously studied materials for CR adsorption. It is evident that the adsorption capacity of the material is considerable, suggesting that it is a promising adsorbent for the removal of the anionic dye.

Table 4.6: The adsorption capacity of the calcined MgZnFe-CO_3 LDH and previously reported materials for CR dye.

Name of adsorbents	Adsorption capacity	References
Calcined MgZnFe-CO_3 LDH	**205.76**	**This work**
Hierarchical $Ni(OH)_2$	151.7	[192]
Hierarchical $NiO - SiO_2$	204.1	[193]
Porous ZrO_2	59.5	[194]
Mesoporous CeO_2	84	[195]
Activated Carbon	189	[196]
Hierarchical $\gamma - AlOOH$	99	[197]
Mg-Al LDH	37.2	[198]
Activated Carbon	300	[199]

4.2.6. Possible adsorption mechanism

It is essential to understand the adsorption mechanism to comprehend the entire adsorption process fully. The adsorption process unfolded through two mechanisms: (1) surface adsorption and (2) anion exchange. In the first mechanism, adsorption occurs on the adsorbent surface through hydrogen bonding and electrostatic interactions. The second mechanism involves replacing anions through the anion exchange process. The complete adsorption process relies heavily on various factors, including the characteristics of the adsorbent and adsorbate, their structural

composition, the presence of functional groups, the interactions between the adsorbent and adsorbate, and the surface properties, all of which play a crucial role [200]. The possible interaction between the CR and LDH is shown in Figure 4.17. Hydrogen bonding, electrostatic interactions, surface diffusion, intra-particle diffusion, n-π

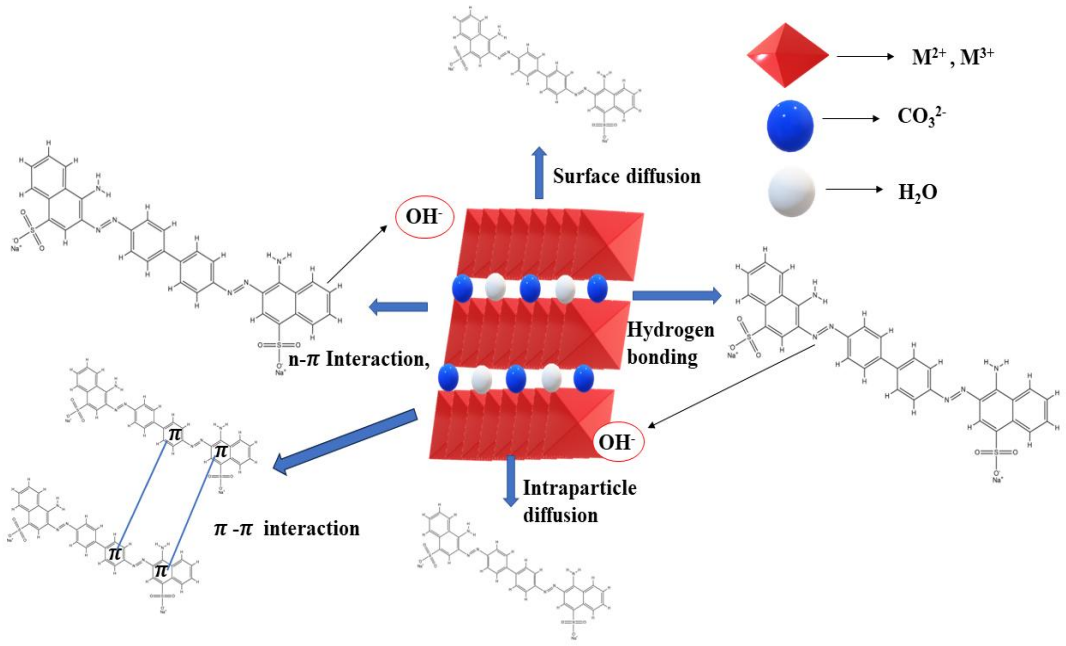

Figure 4.17: Possible adsorption mechanism of Congo-red by MgZnFe-CO_3 LDH.

interactions, and π-π interactions directly influence CR adsorption. The hydrogen bonding between the electronegative group of the CR dye (acting as H acceptors) and the hydrogen atoms of the hydroxyl groups (acting as H donors) has been noted [201]. The n interaction aids in the bonding between OH or oxygen groups on the LDH surface and the aromatic rings of the CR dye, resulting in noncovalent π-π interactions between the aromatic rings of the CR dye [202,203]. Besides chemical bonding, physical adsorption is driven by van der Waals forces, and surface area plays a role in the overall adsorption process. Both uncalcined and calcined LDH, known for their high surface area and porous nature, support the physisorption of CR dye molecules on their external surfaces.

The FTIR analysis was used to investigate the possible adsorption mechanism behind the CR adsorption onto the calcined LDH. Figure 4.18 shows the FTIR spectra of Congo-red and calcined LDH after and before Congo-red adsorption. From figure 4.17, the adsorption band near 1108 cm^{-1} represents the $S = O$ stretching band

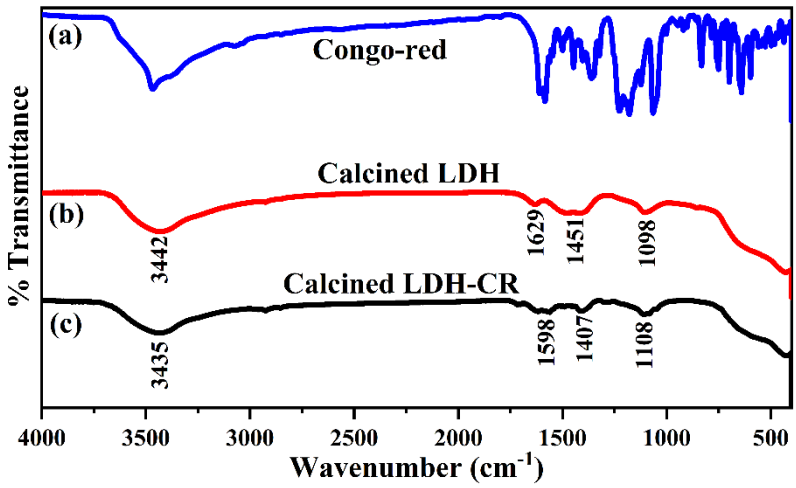

Figure 4.18: FTIR spectra of Congo red, calcined MgZnFe-CO_3 LDH before and after adsorption of Congo-red.

corresponding to Congo-red [204]. This band demonstrated that the calcined LDH successfully adsorbs the CR. The slight shifts in the vibration bands at 3435, 1598, and 1407 cm^{-1} after Congo-red adsorption suggest that the calcined LDH is actively involved in the adsorption. These results suggest that electrostatic interactions and hydrogen bonding formation play a main role in this process.

Therefore, LDH materials are very efficient adsorbents for removing Congo Red from wastewater, owing to their distinctive layered structure, large surface area, and strong electrostatic interactions with anionic dyes. CR dye adsorption onto Layered Double Hydroxides (LDH) is governed by a complex mechanism involving physical and chemical interactions with the LDH surface. LDH, also called hydrotalcite, is a class of anionic clays with a layered structure, making them highly effective in adsorbing anionic dyes like Congo Red.

4.3. Conclusion

In summary, calcined and uncalcined MgZnFe-CO_3 layered double hydroxide was prepared to remove the Congo-red from the aqueous solution. Among these materials, calcined MgZnFe LDH was very efficient in removing the Congo-red. The adsorption was directly correlated with the parameters such as the amount of adsorbent, pH and temperature. Adsorption of Congo-red was analysed using the pseudo-second-order kinetic model, where isotherm kinetics were analysed using the Langmuir isotherm model. The maximum dye adsorption occurred at pH 3; however, all the experimental

procedures were executed at a normal pH of 7. FTIR and SEM analysis indicates that Congo Red adsorption onto the materials was primarily due to electrostatic attraction and hydrogen bonding formation. The adsorption process is endothermic, spontaneous, and highly random, as indicated by the positive value of ΔH_0, the negative value of ΔG_0, and the positive value of ΔS_0.